

Elemental redistribution and Ge loss during ion-beam synthesis of Ge nanocrystals in SiO₂ films

V. Beyer* and J. von Borany

Forschungszentrum Dresden-Rossendorf, Institute of Ion Beam Physics and Materials Research, P.O. Box 51 01 19, D-01314 Dresden, Germany

(Received 9 March 2007; revised manuscript received 29 October 2007; published 23 January 2008)

The elemental redistribution and Ge loss in low-energy Ge⁺ implanted SiO₂ films during wet-chemical cleaning and annealing procedures are investigated. Two effects of major importance for Ge nanocrystal formation have been found. Moisture components (H₂O vapor, H⁺, OH⁻) penetrate into the damaged oxide during storage, wet chemical cleaning, or annealing procedures and lead to a hydrogen and oxygen enrichment in the near-surface oxide. Furthermore, atomic collisions during Ge implantation result in an oxygen excess (with respect to SiO₂ stoichiometry) underneath the Ge profile. The local net ratio of Ge and excess oxygen determines, whether the implanted Ge is incorporated into the SiO₂ network as spatially fixed GeO₂, oxidizes to mobile GeO, or remains as elemental Ge forming nanocrystals. Apart from very shallow profiles, where a drastic Ge loss is observed simply by cleaning in chemical solutions containing H₂O₂, the main Ge loss occurs during annealing. The highly mobile GeO is identified to be responsible for both, Ge redistribution or even loss, if diffusing GeO meets the SiO₂ surface and emanates into the annealing ambient. Annealing in Ar/H₂ mixtures at ≤900 °C reduces the Ge loss due to the reduction of Ge oxides. The enhanced Ge mobility (as GeO) is described as an oxygen vacancy assisted mechanism which also explains the influence of the Si/SiO₂ interface on the Ge diffusivity. Finally, the consequences of Ge redistribution and loss for Ge nanocrystal memory device fabrication are discussed.

DOI: [10.1103/PhysRevB.77.014107](https://doi.org/10.1103/PhysRevB.77.014107)

PACS number(s): 68.55.Ln, 66.30.-h, 61.46.Hk

I. INTRODUCTION

Group-IV (in particular Si or Ge) nanocrystals (NC's) embedded in thin SiO₂ gate dielectrics are of fundamental interest for integrated multidot memory devices.^{1,2} It has been shown that such NC containing thin gate oxides ($d_{\text{ox}} \leq 30$ nm) exhibit charge storage properties with non-volatile (Si NC's) or DRAM-like (Ge NC's) memory behavior.³⁻⁷ The NC's are preferably fabricated by deposition techniques (sputtering, chemical vapor deposition, aerosol spraying) or ion beam synthesis (IBS).⁸ The versatile technology of IBS offers the possibility to generate small clusters (size <4 nm) of different elements (Si, Ge, Au, Sn, Co, etc.) with a high density ($>10^{12}$ cm⁻²) in SiO₂ simply by the variation of the ion species, energy, and fluence of ion implantation.

The IBS process requires an annealing step after ion implantation to recover the damaged oxide and to stimulate the NC's growth. For Ge implanted SiO₂ films this heat treatment is usually associated with two effects of considerable influence on NC's formation: (i) a change of the Gaussian-like implantation profile toward a multimodal Ge distribution and (ii) a partial loss of the implanted Ge amount. Both effects are much pronounced in thin gate oxides when the implanted Ge is located very close to the surface. The redistribution effect has been advantageously used for the formation of a self-organized δ layer of Ge NC's in vicinity to the Si/SiO₂ interface,^{3,9-12} which is a desired configuration to achieve multidot memories with low programming voltages and/or times.

For thick SiO₂ films ($d_{\text{ox}} > 100$ nm) the influence of implantation and annealing conditions on the Ge redistribution has been studied by numerous investigations,^{10,13-19} however, the detailed mechanism remains under discussion. It is

widely accepted that both, redistribution and loss are strongly influenced by moisture contaminants (H₂O, OH, H₂) which penetrate the damaged oxide after ion implantation.²⁰ These species originate either from air humidity and wet cleaning chemicals ("intrinsic source") or from the residual moisture in the "inert" Ar or N₂ annealing ambient ("extrinsic source"). During annealing the excess oxygen and hydrogen may react with Ge leading to the formation of amorphous GeO₂ and mobile (volatile) compounds such as GeH₄ or GeO. In detail, the effect of Ge oxidation during annealing was studied by Heinig *et al.*¹⁵ and Borodin *et al.*¹⁶ for 500 nm SiO₂ films. Their kinetic three-dimensional (3D) lattice Monte Carlo (KLMC) simulations consider the diffusion of two kinds of interacting impurities—dissolved Ge monomers and an oxidizing component (e.g., O₂, OH). The simulated Ge redistribution and the formation of near-surface GeO₂ are in good agreement with the experimental results obtained by x-ray photoelectron spectroscopy (XPS) and transmission electron microscopy (TEM). However, as the GeO₂ is spatially fixed, any Ge loss cannot be explained by this model. The considerable loss (~50%) after a furnace annealing of Ge implanted SiO₂ films at $T=1100$ °C in Ar+7% H₂ found by Markwitz *et al.*^{14,21} was attributed to volatile GeH₄ or GeO but no experimental evidence has been reported.

In this paper the Ge redistribution and loss are studied for low-energy implanted SiO₂ films where the Ge is located in a very near-surface region (≤ 20 nm). This is of particular interest for the synthesis of Ge NC's in thin gate oxides being designed for memory devices. In addition to the variation of the ion energy and fluence, experimental conditions were selected that allow the separation of effects from cleaning and annealing. Based on the experimental results a

TABLE I. Implantation and annealing parameters. For different implantation energies the fluences were adjusted to ensure a uniform maximal Ge content of approximately 7 or 17 at. % for the LD or HD implants, respectively.

Series	SiO ₂		Ion Implantation			Annealing
	<i>d</i> _{ox} (nm)	Ion	<i>E</i> (keV)	LD (cm ⁻²)	HD (cm ⁻²)	
A	1000	⁷⁴ Ge	1.5	1.8 × 10 ¹⁵	5.1 × 10 ¹⁵	Ar (9.0) 600–1050 °C 30s/10 min
			3	2.4 × 10 ¹⁵	6.8 × 10 ¹⁵	
			6	3.4 × 10 ¹⁵	9.5 × 10 ¹⁵	
			12	4.9 × 10 ¹⁵	1.4 × 10 ¹⁶	
B	100	⁷⁴ Ge	12		1.8 × 10 ¹⁶	Ar(9.0)/ Ar+5% O ₂ / Ar+5% H ₂
					1.8 × 10 ¹⁶	
	50	⁷⁴ Ge	12		1.8 × 10 ¹⁶	900 °C/ 1000 °C, 5 min
				²⁸ Si	200	

qualitative discussion of the mechanisms and chemical processes involved in the Ge redistribution and loss is given.

II. EXPERIMENT

A. Sample processing

Low-energy implantations of ⁷⁴Ge⁺ ions ($E \leq 12$ keV) were carried out at room temperature into 1 μm, 100 nm, or 50 nm SiO₂ films thermally grown on Si(100) substrates. The implantation parameters are summarized in Table I. Different energies (1.5–12 keV) and two fluences [low/high fluence: LD/HD, labeled after the more technical terms “low dose” and “high dose”] were used to investigate the depth and concentration dependence on the Ge redistribution and loss. After ion implantation a common wet-chemical cleaning step in H₂O₂/H₂SO₄ (CP1) was performed (see Table II). A cleaning is necessary before annealing to remove possible surface contaminations from implantation handling. The influence of different chemical components during the prean-

TABLE II. Process sequence and parameters of the wet-chemical H₂O₂/H₂SO₄ cleaning treatment (CP1) and the modified cleaning procedures (CP2–CP4).

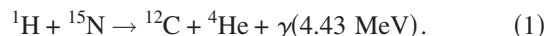
	Step 1	Step 2	Step 3	Step 4
Process sequence	Boiling H ₂ O ₂ /H ₂ SO ₄	Ultrasonic Deionized H ₂ O	Ultrasonic Isopropanol (C ₃ H ₈ O)	Drying N ₂ flow
	120 °C 10 min	20 °C 10 min	20 °C 1 min	20 °C
	CP1			
	CP2 (step 1 without H ₂ O ₂)			
		CP3		
			CP4	

neal cleaning treatment was investigated separately for samples implanted with the lowest energy ($E=1.5$ keV). Here, the cleaning sequence has been stepwise reduced as described in Table II.

Rapid thermal annealings (RTA) were carried out at temperatures between 600 and 1050 °C in different atmospheres for times between 30 s and 10 min. In most cases, the annealing was performed in an ultrapure “inert” Ar ambient (purity 9.0 with respect to O₂, OH) by using an Aeronex gas purifier. For these conditions, the influence of the “extrinsic source” on the Ge redistribution can be neglected. For comparison, a few anneals were performed in gas mixtures of Ar+5% O₂ or Ar+5% H₂ to stimulate the impact of oxygen or hydrogen. Thus, the separation of effects related to the penetration of moisture before annealing or from the annealing ambient is possible. In a separate experiment, Si ions were implanted (200 keV/1 × 10¹⁶ cm⁻²) prior to Ge to study the influence of an additional deep oxide damage—where a higher amount of penetrated moisture in the oxide can be suggested—on the Ge loss and redistribution.

B. Analysis techniques

The content and depth distribution of Ge in SiO₂ was traced by Rutherford backscattering spectrometry (RBS) using 1.2 MeV He ions (series B: 1.7 MeV) at a scattering angle of 170°. To improve the depth resolution an incidence angle of typically 70° (series B: 60°) perpendicular to the surface normal was used. The penetration of hydrogen or hydrogen containing species (H₂O, OH⁻, H⁺) into the damaged SiO₂ after implantation and cleaning was detected by means of nuclear reaction analysis (NRA) using the resonance reaction



Details of this technique and the data evaluation are described elsewhere.²² The chemical state of Ge was analyzed by XPS. The measurements were performed by a Microlab 310F (Fisions) spectrometer using a Mg x-ray tube ($E=1254$ eV). The inelastic mean free path of photoelectrons in SiO₂ is ≤ 3.3 nm (Ref. 23) which determines the XPS information depth. Within this study the XPS analysis is restricted to samples implanted with the lowest energy ($E=1.5$ keV) to exclude any influence of the sputtering process during depth profiling on the chemical information.²⁴ The XPS spectra are calibrated in energy and intensity to the C1s peak (285.0 eV) and the O2s signal, respectively. The latter is dominated by oxygen from the SiO₂ network and is thus considered as a reference.

III. RESULTS AND DISCUSSION

Figure 1 shows the Ge implantation profiles and the corresponding damage distributions as calculated by TRIDYN (Ref. 25) and SRIM (Ref. 26), respectively. Depending on the energy, the projected range R_p varies between 4 nm ($E=1.5$ keV) and 13 nm ($E=12$ keV). The slight decrease of the peak concentration with energy (compared to uniform 7 and 17 at. % for LD and HD, respectively, as estimated by

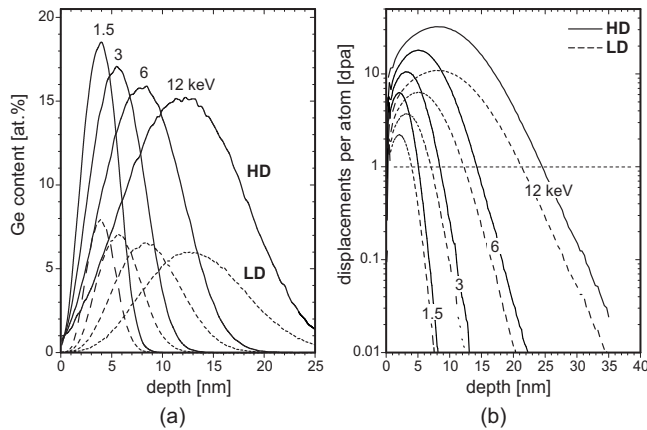


FIG. 1. (a) Ge profiles according to the implantation parameters of Table I, series A; (b) Corresponding damage distribution in terms of the dpa rate. The HD and LD profiles are plotted with closed and dashed lines, respectively.

SRIM, see Table I) is related to changes in the matrix composition during implantation included in the TRIDYN calculation. Effects of sputtering and oxide swelling are negligible (LD) or compensate each other (HD); thus, for each energy the position of the Ge peaks is independent of the fluences. The damage calculation [Fig. 1(b)] reveals that the near-surface displacement-per-atom (dpa) rate is always ≥ 1 , i.e., each atom in the oxide matrix is displaced at least once on an average during implantation. About 70% of the implanted Ge is located within the region of strongly damaged oxide (defined by $\text{dpa} > 0.3$) between 6 and 16 nm depending on the energy. For samples of series A both the impurity and the damage profiles are far away from the Si substrate, which avoids any influence of the Si/SiO₂ interface on the Ge redistribution and loss.

A. Ge loss during wet-chemical cleaning

As shown in Fig. 2(a), already a standard wet-chemical H₂O₂/H₂SO₄ cleaning treatment (CP1) after ion implantation reduces significantly the Ge content in SiO₂. The Ge loss increases with decreasing implantation energy, i.e., the closer the implanted Ge is located to the surface. For a shallow Ge implant of 1.5 keV, $5 \times 10^{15} \text{ cm}^{-2}$ ($R_p = 4 \text{ nm}$) almost all Ge gets lost after CP1 cleaning. A separation of the different steps involved in the cleaning sequence clearly reveals that the H₂O₂ component determines the Ge loss during cleaning [Fig. 2(b)]. An ultrasonic flushing in deionized water or in hydrocarbon solvents (such as isopropyl alcohol) solely have only a minor influence on the Ge loss. A cleaning treatment similar to CP3 but with boiling water ($\sim 100 \text{ }^\circ\text{C}$) in step 2 reproduces the result of CP2 which excludes a crucial influence of the cleaning temperature.

The significant Ge loss during H₂O₂/H₂SO₄ (CP1) cleaning can be explained as follows: During implantation nearly all Si and O atoms within a near-surface oxide region are displaced due to atomic collisions [Fig. 1(b)], which is associated with bond reconfigurations. The as-implanted Ge are bound preferably to oxygen atoms from the disturbed matrix

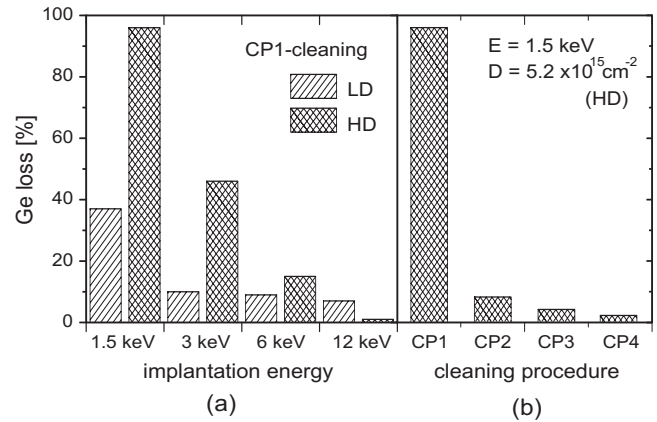


FIG. 2. Loss of Ge due to wet-chemical cleaning treatment obtained from RBS data (not shown) using the as-implanted sample as a reference. (a) Ge loss after a standard H₂O₂/H₂SO₄ cleaning procedure before annealing. (b) A stepwise investigation of the complete cleaning sequence isolates the H₂O₂ as the main component responsible for the Ge loss during cleaning.

or additional oxidizing species (O₂, OH, etc.) penetrating into the damaged oxide after implantation. XPS studies showed that Ge bulk material exposed to air oxidizes to GeO₂ at the surface (oxidation state Ge⁴⁺) (Refs. 27–29), whereas a mixture of different oxidation states (Ge⁰, Ge²⁺, Ge⁴⁺) is observed for Ge implanted ($E > 100 \text{ keV}$, $R_p > 70 \text{ nm}$) thick SiO₂ films.^{17,30,31} In our experiments, XPS of low-energy (1.5 keV) implanted samples (see Figs. 3 and 5) confirm GeO₂ (Ge⁴⁺) as the dominant oxidation state of Ge. This is not surprising as the main part of the Ge is located in a very-near surface region $\leq 3 \text{ nm}$ [see Fig. 1(a)]. Ge oxides or hydroxides differ with respect to their solubility in water: GeO or Ge(OH)₂ (Ge²⁺) are more or less insoluble whereas GeO₂ (Ge⁴⁺) has a high solubility.³² H₂O₂ is a strong oxidizing reagent. In general, a cleaning procedure, which involves H₂O₂, transforms near-surface Ge, GeO, Ge(OH)₂ (Ge⁰, Ge²⁺) or similar components to GeO₂ (Ge⁴⁺) and solute this oxide in H₂O [from H₂O₂ → H₂O + (1/2)O₂] by forming H₂GeO₃.³² It has been shown³³ that the presence of oxygen is of vital importance for the dissolution of Ge in aqueous solutions. Although the oxidation state Ge⁴⁺ is already the major configuration after implantation and storage at humid air (Fig. 3), only minor Ge loss is obtained after flushing in cold or boiling H₂O contrary to a H₂O₂ treatment. This result indicates that the solution of GeO₂ embedded in the SiO₂ matrix (despite damage) differs from those of natively oxidized Ge surfaces. It is obvious to assume that this difference is related to existing Ge—O—Si bonds, which do not allow an efficient solution in pure water. Oxygen radicals from decomposing H₂O₂ provide a high amount of reactive oxygen to form H₂GeO₃. The process starts at the surface and proceeds into depth, creating a porous structure due to the selective removal of solvated Ge. As a higher Ge content enables a better chemical attack, the Ge loss increases with implantation fluence [Fig. 2(a)].

B. Ge loss during annealing

During annealing a further Ge loss is obtained. As shown in Fig. 4 the Ge content decreases with annealing tempera-

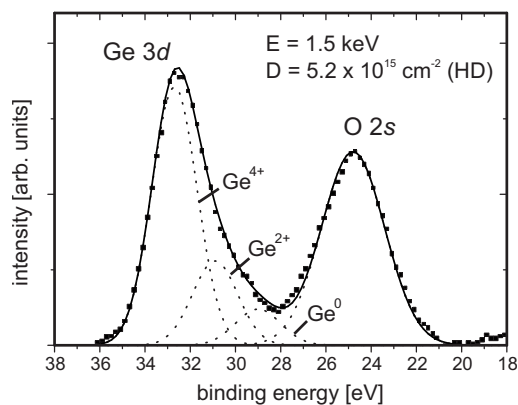


FIG. 3. XPS Ge 3*d* and O 2*s* data for the 1.5 keV, HD implant (as implanted). The Ge 3*d* peak reveals a mixture of GeO₂ (Ge⁴⁺), GeO (Ge²⁺), and Ge (Ge⁰) compounds (dotted) with binding energies of 32.7, 30.9, and 29.0 eV, respectively, which is about 0.9 eV per Ge—O bond (see Refs. 27, 29, and 30). The O 2*s* peak centered at 24.8 eV corresponds mainly to oxygen from the SiO₂ network.

ture, which indicates a thermally activated, i.e., reaction and/or diffusion controlled process of Ge loss. A higher percentage of Ge remains for a higher implantation depth. The fluence dependence becomes more significant the closer the Ge is located to the surface [Fig. 4(b)]. With a higher thermal budget the absolute Ge loss saturates at a level of about 4×10^{15} and 8×10^{15} cm⁻² for the LD and HD samples, respectively, if enough Ge is available. For the 1.5 keV, LD implant the residual Ge content decreases from 62% after cleaning to 40% of the initial amount already after annealing at 600 °C for 10 min. As shown in Fig. 5 in this case only fully oxidized Ge (GeO₂, Ge⁴⁺) and elemental Ge (Ge⁰) remain after annealing. Thus, the Ge loss during annealing is attributed to intermediate Ge—O compounds with a mean binding energy of about 31.7 eV (see Ref. 27). This corresponds, e.g., to a Ge³⁺ configuration, i.e., to Ge connected to three oxygen atoms with one dangling or Ge—Ge (Ge—Si) bond.

The Ge loss during annealing is supposed to be due to the formation of volatile Ge compounds, i.e., GeH₄ or GeO. To form these compounds, excess hydrogen or oxygen atoms are required nearby the implanted Ge. Two sources of excess oxygen and hydrogen can be defined. Firstly, ion implantation damages the oxide in a way that adsorbed water from humid air at the surface is able to penetrate the oxide by H₂O or (after dissociation) by OH⁻ and H⁺/H₃O⁺ molecules.^{20,34} The irradiation causes the formation of strained three-membered ring structures in the SiO₂ network, which are not stable for aqueous solutions.^{35,36} The near-surface hydrogen (and oxygen) enrichment in the oxide after ion implantation is verified by NRA as shown in Fig. 6 for marginal implantation parameters. The hydrogen content decreases in depth in a diffusionlike manner without any visible accumulation in the region of the implanted Ge. The penetration depth (or the decay) is just correlated to the implantation energy, i.e., the depth of the modified oxide. The hydrogen profile is only weakly affected by the wet chemical cleaning treatment, thus

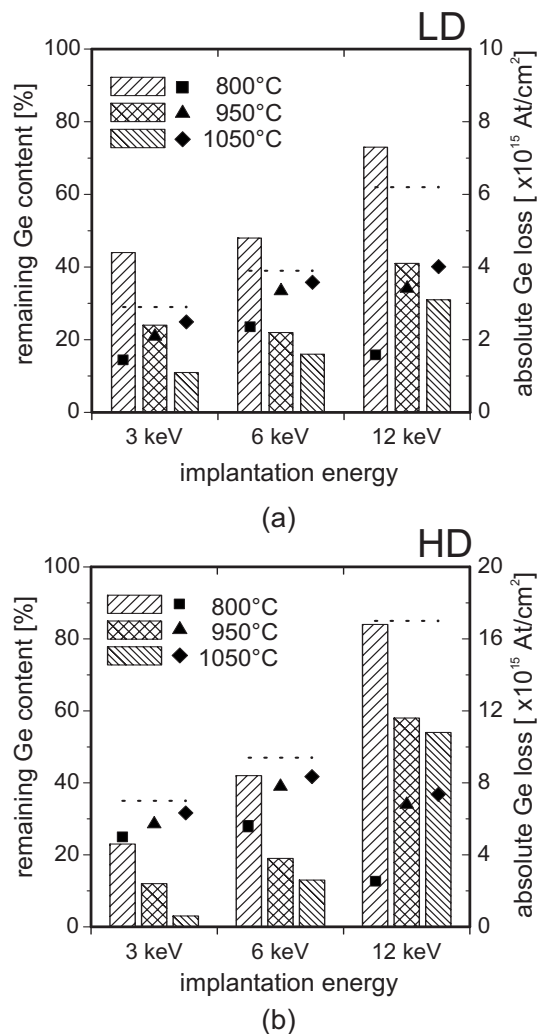


FIG. 4. Ge loss after RTA treatments in pure Ar for 30 s for LD (a) and HD (b) implants at energies between 3 and 12 keV (series A). The bar graphs belong to the left ordinate showing the remaining Ge content relative to the value after H₂O₂/H₂SO₄ cleaning. The corresponding absolute Ge loss and the implanted fluence are indicated by symbols and a dotted line, respectively (right ordinate). The RBS measurements reveal minor differences between the implanted fluence and the initial parameters (see Table I).

the oxide is already conditioned after exposition to humid air subsequent to ion implantation. Secondly, the collision cascade and preferential sputtering during Ge implantation leads to local changes in the elemental oxide composition with respect to the SiO₂ stoichiometry. This process is only associated to oxygen-related effects on the Ge loss and redistribution, whereas the penetration of additional hydrogen and oxygen (from humidity or as contaminants in the annealing ambient) into the oxide have to be considered to both Ge oxide and hydride formations.

In the following exemplarily for the 12 keV Ge implants, where the highest remaining Ge contents are obtained in Fig. 4, the effects of excess oxygen and hydrogen on the loss and redistribution of Ge will be discussed in detail. The RBS data in Figs. 7(a) and 8(a) reveal that after annealing in pure Ar the Ge gets lost mainly from a region behind the profile

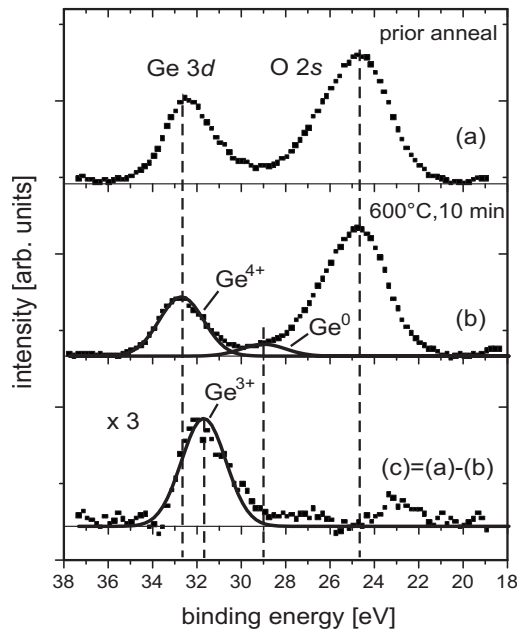


FIG. 5. XPS Ge 3d and O 2s data prior to (a) and after annealing at 600 °C, 10 min (b) for 1.5 keV, LD implantation. The difference spectrum (c) of disappearing Ge during annealing is attributed to Ge³⁺ (31.7 eV).

maximum (HD) or rather homogeneously (LD) depending on the implantation fluence. The oxygen excess related to moisture is deduced from NRA data (Fig. 6) assuming a ratio H:O=2:1. As calculated by TRIDYN, atomic collisions during ion implantation lead to an oxygen deficit close to the surface and an oxygen accumulation behind the implanted Ge profile [Fig. 7(b)]. Thus, the net oxygen excess can be calculated as presented in Figs. 7(a) and 8(b). The oxygen from moisture preferably saturates empty Si bonds and compensates the O deficit in the first 15 nm oxide depth for SiO₂ reconstruction during annealing. This process inhibits the

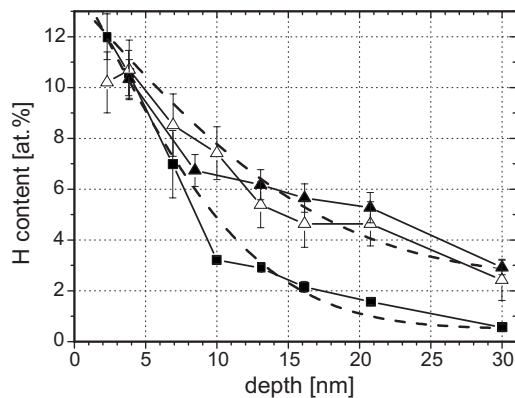


FIG. 6. Hydrogen depth profiles in SiO₂ obtained by NRA after ion implantation at 1.5 keV, LD (■) and 12 keV, HD (▲), the latter also after standard cleaning (△). Fitted profiles assuming a diffusionlike penetration [using the function $N(x)=N_0 \operatorname{erfc}(x/2k)+c$ with the fitting parameter N_0 , k , and c] are shown by dashed lines. A standard as-grown thermal oxide contains less than 0.5 at. % H (Ref. 20).

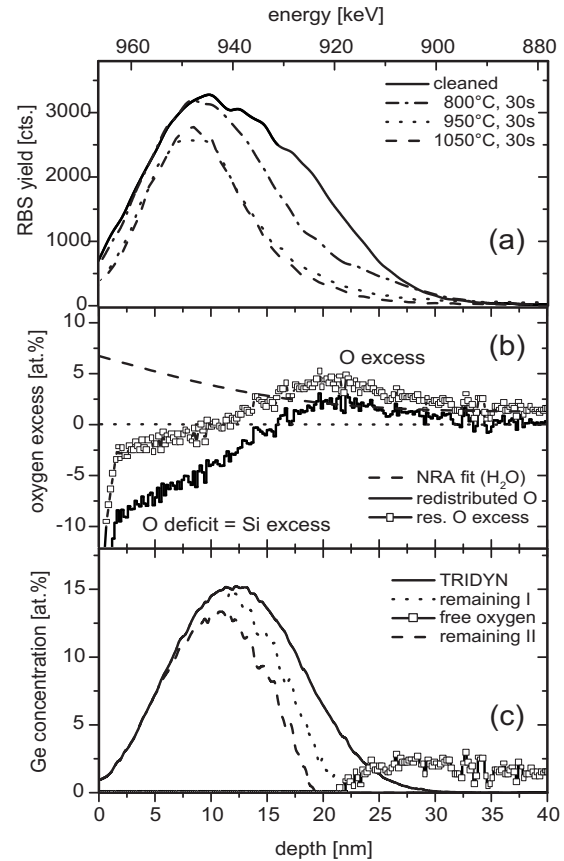


FIG. 7. Depth dependence of Ge loss during annealing for 12 keV, HD Ge implantation. (a) Ge profiles for different annealing temperatures as measured by RBS. (b) Total oxygen excess (squares) from a superposition of oxygen from H₂O in-diffusion (dashed line) as obtained from NRA measurements (Fig. 6) with those—deficit or excess—generated during Ge implantation (straight line). (c) Profile changes (dotted line) due to a Ge loss by the formation of GeO with respect to the oxygen profile from (b) starting from the simulated implantation profile (straight line) [see Fig. 1(a)]. Remaining free oxygen (squares) according to the static approach causes further reduction of the Ge content during annealing (dashed line), which is considered to be more effective at the rear of the Ge implantation profile with a linearly decreasing impact toward the oxide surface.

formation of Ge oxides because SiO_{2(s)} has a much higher heat of formation ($\Delta_f H^\circ = -910.7 \text{ kJ/mol}$) than GeO_{2(s)} ($\Delta_f H^\circ = -580 \text{ kJ/mol}$) or GeO_(s) ($\Delta_f H^\circ = -262 \text{ kJ/mol}$).³⁷ Only the net oxygen excess—obtained mainly behind the Ge profile in Fig. 7(b)—is supposed to react with the implanted Ge impurity atoms to form GeO during annealing. This GeO is mobile at elevated temperatures and escapes from the oxide surface toward the annealing ambient²⁷ (Ge loss) due to its high vapor pressure (about 1 mbar at 700 °C).^{38–40} In a static balance of the calculated Ge content and the net oxygen excess the spatial Ge distribution changes as shown in Figs. 7(c) and 8(c) (denoted “remaining Ge I”). Such static approximations—both Ge and O are considered as locally fixed also during annealing—are likely in case of an oxygen deficient oxide as after implantation. Oxygen (and hydrogen)

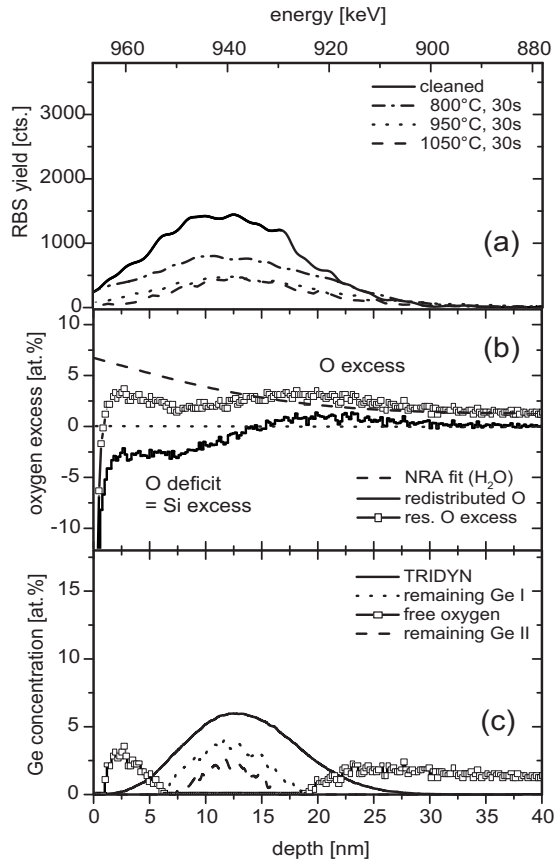


FIG. 8. Depth dependence of Ge loss during annealing for 12 keV, LD Ge implantation (notations as in Fig. 7). In (c) a homogeneous reaction is considered for simplicity, as “free oxygen” is available from both sides of the Ge profile.

are presumably bound to Si and Ge forming $\equiv\text{Si}-\text{OH}$ (Ref. 41) or $\equiv\text{Ge}-\text{OH}$ bonds (accordingly $\equiv\text{Si}-\text{H}$ and $\equiv\text{Ge}-\text{H}$) (Refs. 42–44) or being attached as H_2O (Ref. 45). However, some additional excess oxygen exists labeled as “free oxygen” in Figs. 7(c) and 8(c). This oxygen can be considered to be neither connected to Ge nor to Si in the SiO_2 network and is thus quite mobile during annealing. During diffusion toward the surface it reacts to remaining Ge or excess Si and reduces the Ge content further as indicated by “remaining Ge II” in Figs. 7(c) and 8(c). This estimation represents an upper limit of loss assuming the implanted Ge as the dominant sink for oxygen. For a lower Ge loss some oxygen might have left the oxide toward the ambient or is trapped at the Si bulk in the other diffusion direction. As a consequence, only the remaining Ge content is available for NC formation and determines the size and density of the corresponding NC’s.

The model of GeO formation and emanation clearly reproduces the changes of the Ge profile shape after annealing as measured by RBS Figs. 7(a) and 8(a). Note that the RBS depth profiles are superposed by the Si detector resolution [full width at half maximum (FWHM) ≈ 15 keV] leading to a broadening of the Ge distribution. Furthermore, the calculated Ge losses are in reasonable agreement with the experimental values (LD/HD: calculated 83/33 %, exp. 69/45 %),

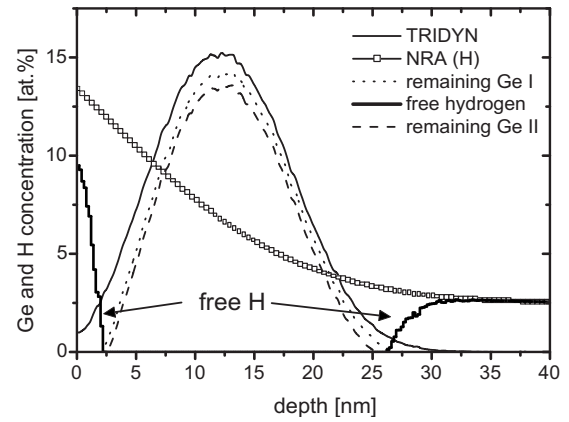
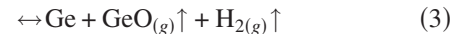
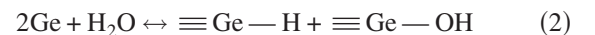


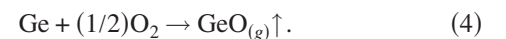
FIG. 9. Ge loss and redistribution due to GeH_4 formation simulated for the 12 keV, HD Ge implant. The initial hydrogen concentration (squares) is taken from NRA (Fig. 6). The simulation reveals negligible profile changes for both the static and diffusion approximations. The initial Ge distribution is calculated by TRIDYN (straight line).

which confirms the main assumptions of the model.

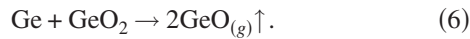
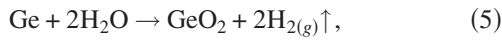
A similar calculation can be performed for a hydrogen related loss assuming the formation of volatile GeH_4 instead of GeO (see Fig. 9), but due to the $\text{Ge}:\text{H}=1:4$ ratio the expected Ge loss is much lower ($\leq 20\%$) and does not reproduce the changed profile shape. In addition, from thermodynamics the formation of $\text{GeO}_{(g)}$ ($\Delta_f H^\circ = -46.2$ kJ/mol) is favored compared to $\text{GeH}_{4(g)}$ ($\Delta_f H^\circ = +90.8$ kJ/mol) (Ref. 37) during annealing if both reaction pathways are possible. Considering in the calculation only an effect due to penetrating H_2O , the loss related to oxygen would be approximately twice that of hydrogen. Differences are caused by the redistributed oxygen from ion implantation, which changes considerably the depth profile of excess oxygen in comparison to hydrogen. In summary the following reactions occur during annealing in pure Ar leading to the formation of volatile GeO. For moisture components ($\text{H}_2\text{O} \leftrightarrow \text{H}^+ + \text{OH}^-$)



and for O excess caused by recoils



The reactions stop if all excess O is consumed, which is considered to be the reason for the saturating Ge loss for higher annealing temperatures [see Fig. 4(b)]. These considerations hold primarily for systems where the content of Ge in SiO_2 considerably exceeds the amount of reactive oxygen. Otherwise, as for 1.5 keV Ge implantation, the formation of GeO_2 is much more probable (see Figs. 3 and 5), which is completely miscible with SiO_2 . In the case where Ge NC’s are formed and just partially oxidized or passivated by a GeO_2 shell, a reduction might occur during annealing in oxygen deficient ambient by the formation of volatile GeO:^{27,28,32}



As previously demonstrated in this paper, the Ge loss is mainly determined by the amount and distribution of excess oxygen with respect to the position of the implanted Ge profile. Due to the strong influence of implantation and annealing parameters, an estimation of the Ge loss requires a modeling based on the most relevant processes with detailed knowledge of the experimental conditions. From the diffusionlike moisture distribution in SiO_2 as obtained by NRA a dominating Ge loss close to the SiO_2 surface would be expected. However, in this region Ge is stabilized by an O-deficient oxide which consumes a significant part of the penetrating oxygen for the recovery of the SiO_2 network. The formation of small Ge precipitates or NC's in SiO_2 suppresses the Ge loss due to the self-limiting oxidation of small particles.⁴⁶ This might contribute to a smoother profile of the remaining Ge, but is not able to avoid the Ge loss in general.

C. Influence of annealing ambient and extended oxide damage

In the previous subsection due to annealing in ultrapure Ar, we were able to investigate solely the role of the “intrinsic source” (caused by the penetration of moisture after ion implantation) on the Ge loss and redistribution. Reactive species introduced by the annealing ambient had been excluded. In the second set of samples (series B, $d_{\text{ox}} \leq 100$ nm) the annealing ambient has been enriched by a small amount of oxygen or hydrogen (see Table I) to stimulate the corresponding effects compared to annealing in ultrapure Ar. The Ge implantation was performed at 12 keV, $1.8 \times 10^{16} \text{ cm}^{-2}$, which is close to the 12 keV HD implant of the preceding experiment (series A).

As shown in Fig. 10(a) annealing in pure Ar at 900 °C for 5 min leads again to a considerable Ge loss (60%) with similar changes in the Ge profile shape as obtained before [see Fig. 7(a)]. Annealing in an oxygen containing ambient (Ar+5% O_2) causes a clear Ge redistribution toward the surface with a slightly lower total loss of about 40% of the initial Ge amount, whereas additional hydrogen (Ar +5% H_2) significantly reduces the loss to about 17%. In agreement with previous investigations^{14–17} for annealing in oxygen containing atmosphere, GeO_2 has formed in a region close to the surface where the profiles of in-diffusing oxygen and out-diffusing Ge species (mainly GeO) overlap during annealing. An oxidation to GeO_2 fixes the volatile GeO within the oxide and reduces the total Ge loss:



In case of the formation of volatile GeH_4 in SiO_2 a much enhanced loss was expected during annealing in Ar+ H_2 , but contrariwise Ge seems to be immobilized in the presence of hydrogen at least for 900 °C annealing. About the reason for this behavior one can just speculate considering the present experimental data. With respect to moisture related loss [Eq. (2)], Ge—O compounds such as $\equiv\text{Ge—OH}$ can be reduced

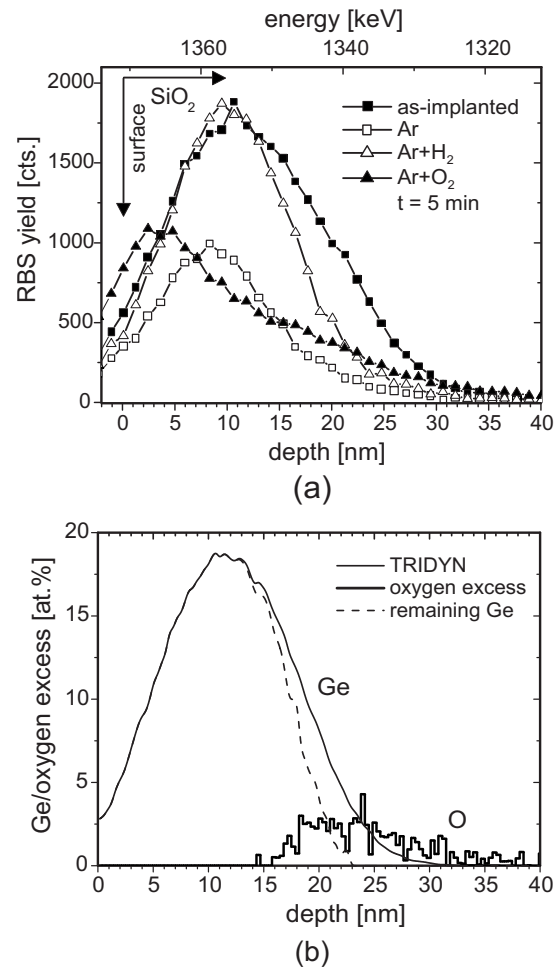
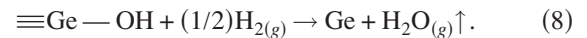


FIG. 10. (a) Ge distribution after annealing in Ar/ H_2 or Ar/ O_2 mixtures at 900 °C for 5 min obtained by RBS. (b) Changes in the Ge profile taking only displaced oxygen during implantation into account. The data for the Ge content and O excess are obtained by TRIDYN calculations.

by hydrogen to elemental Ge under emanation of H_2O :⁴⁷



On the other hand, the balance reaction in Eq. (3) might be weighted to the left side due to a significant partial pressure of H_2 in the oxide, which suppresses the formation of GeO by hindered release of gaseous H_2 . In both cases the Ge loss due to the moisture related oxygen excess will be reduced. Assuming solely recoiled oxygen, the respective calculations illustrated in Fig. 10(b) validate the experimental results. The calculated Ge loss of 12% is very close to the experimental value of 17%, also corresponding to profile changes. The recoiled excess oxygen oxidizes local Ge to GeO , which is apparently not affected by H_2 at 900 °C. It seems to be plausible that a single weak Ge—OH bond (moisture) can be more easily released by hydrogen than stronger Ge=O bonds (displaced oxygen).

In a different experiment a sequential 200 keV Si and 12 keV Ge implantation was carried out in 100 nm SiO_2 (see Table I) without breaking the vacuum condition during im-

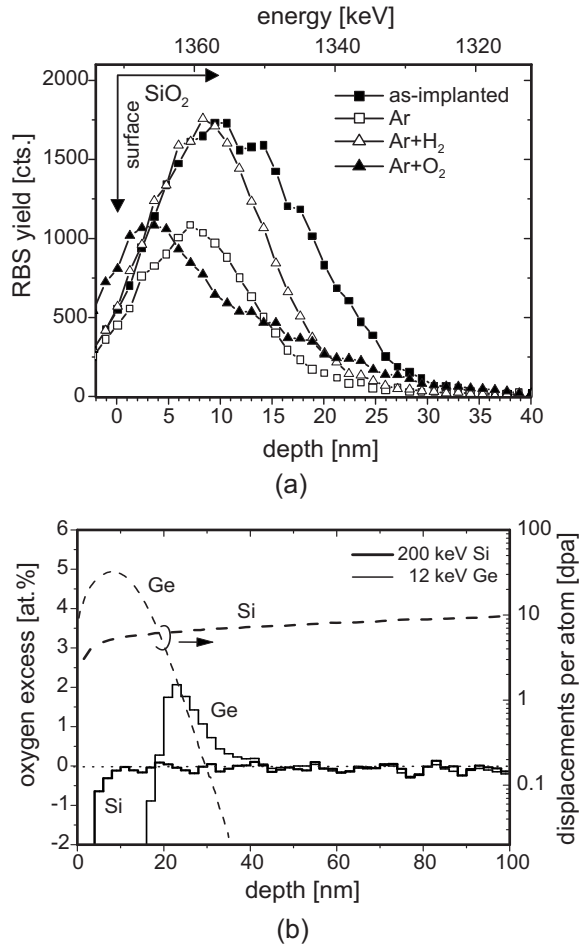


FIG. 11. (a) Ge distribution obtained by RBS for a consecutive 200 keV Si ($R_p=280$ nm) and 12 keV Ge implantation in 100 nm SiO₂ (series B) after annealing at 900 °C for 5 min in different ambients. (b) TRIDYN simulation of the Si/Ge implantations according to stoichiometry changes between the Si and O (oxygen excess). The dpa rate during implantation (dashed lines) is also shown and refers to the right ordinate.

plantation. As shown in Fig. 11(b) the number of dpa's exceeds about 5 across the whole oxide, whereas the content of implanted Si remains negligible (≤ 0.1 at. %). One could assume that a homogeneous irradiation of the entire oxide layer forces the penetration depth of moisture. However, as illustrated in Figs. 11(a) and 10(a), independent of the annealing ambient, almost the same Ge loss and redistribution are obtained after annealing in comparison to films without Si irradiation. The homogeneous oxide damage from the Si irradiation has apparently no impact on the total moisture content within the oxide. As shown in Fig. 11(b) the oxygen redistribution from atomic collisions during Si irradiation is negligible compared to the subsequent Ge implant. Thus, the penetration of moisture seems to be more related to the depth of substoichiometric oxide as generated by Ge implantation, which reflects a higher amount of Si dangling bonds, than to the total number of dpa's [Fig. 11(b)]. Thus, the diffusionlike moisture profile in ion-irradiated SiO₂ might saturate even for a deeper oxide damage at a level similar to the hydrogen

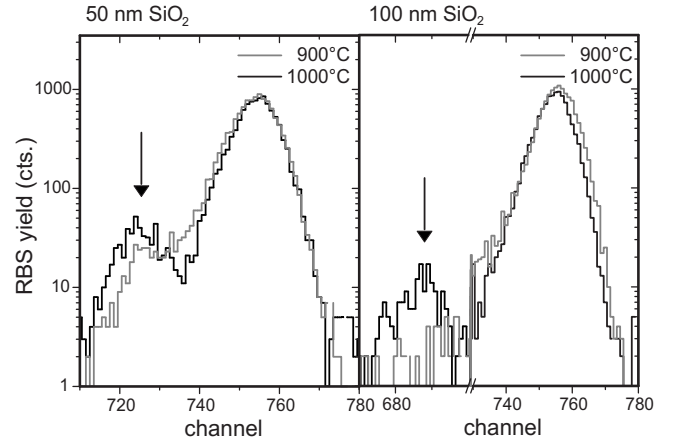


FIG. 12. Ge profiles from RBS after combined Si and Ge implantation in 50 nm (left) and 100 nm (right) SiO₂ films, annealed in pure Ar at 900 and 1000 °C for 5 min (series B). A distinct Ge amount is trapped at the Si/SiO₂ interface (marked by arrows). Nearly the same results were obtained for a single Ge implantation in 100 nm SiO₂ without Si irradiation.

depth profile in Fig. 6 for 12 keV implantation.

IV. DIFFUSION OF Ge AND GeO IN SiO₂

A. Activation energy of diffusion

In addition to mobilized Ge due to GeO formation there is no broadening of the remaining Ge profile as shown, e.g., in Fig. 10(a) for annealing in Ar+H₂. This clearly indicates that for $T \leq 1000$ °C elemental Ge has apparently a much lower mobility in SiO₂ than GeO. From our experiments a diffusion coefficient of $D \ll 10^{-16}$ cm²/s at 900 °C can be estimated. For substitutional Ge in amorphous silica glass, Minke and Jackson⁴⁸ determined the diffusivity to $D(900 \text{ °C}) = 2.6 \times 10^{-21}$ cm²/s and $D(1000 \text{ °C}) = 2.2 \times 10^{-19}$ cm²/s ($D_0 = 7250$ cm²/s; $E_A = 5.69$ eV), which enables a diffusion length of only a few nanometers for $T = 1000$ °C. It is noteworthy that the activation energy for the self-diffusivity of Si in SiO₂ films is close to that value [$E_A = 5.34$ eV (Ref. 49)] which indicates an unique diffusion mechanism probably slightly influenced by the different atomic radii (Si: 1.46 Å, Ge: 1.52 Å).

More detailed information concerning the activation energy for the diffusion of GeO can be derived from the Ge accumulation after annealing at the Si/SiO₂ interface as shown in Fig. 12. This accumulation is a common effect in Ge implanted SiO₂ films^{13,15} caused by a condensation of Ge and O from diffusing GeO at the substrate surface according to Eq. (9):



During annealing time t_a an areal density $m(T, t_a)$ of Ge atoms is trapped at the Si/SiO₂ interface, more precisely at the uppermost atomic layers of the Si substrate, in a distance Δx to the Ge profile. Accordingly, there the Ge concentration is initially $N_0 = 0$ with a constant gradient toward the Ge profile of $\Delta N(T) = N(T) - N_0$, i.e., no Ge is re-emitted from the Si

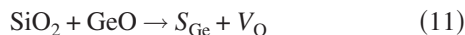
substrate into the oxide. Assuming an uniform diffusion coefficient $D \neq D(x)$, a linearization of Fick's first law yields

$$m(T, t) = D(T) \frac{\Delta N(T)}{\Delta x} t_a = \tilde{D}_0 \exp\left(-\frac{E_A}{kT}\right) \frac{t_a}{\Delta x}. \quad (10)$$

The atomic concentration $N(T)$ of the diffusing Ge specie close to the Ge profile depends on the heat of formation for the corresponding chemical reaction. Thus, the total activation energy E_A includes both, the energy of formation and migration; \tilde{D}_0 is an effective prefactor of diffusion (unit: 1/cms). From the RBS data in Fig. 12 in case of implantation in the 50-nm-thick oxide $m(900^\circ\text{C}) = 1.6 \times 10^{14} \text{ cm}^{-2}$ and $m(1000^\circ\text{C}) = 3.4 \times 10^{14} \text{ cm}^{-2}$ can be easily deduced, resulting in $E_A \approx 0.95 \text{ eV}$. For 100-nm-thick SiO_2 $m(900^\circ\text{C}) \leq 3 \times 10^{13} \text{ cm}^{-2}$ and $m(1000^\circ\text{C}) = 1.0 \times 10^{14} \text{ cm}^{-2}$ are obtained, but the first value indicates just an upper level as the amount of trapped Ge is below the detection limit. A respective activation energy of $E_A \geq 1.55 \text{ eV}$ indicates that the diffusivity of GeO is clearly influenced by the Si/SiO₂ interface whereas E_A increases with the distance of the Ge profile to the interface. A similar effect of the oxide thickness is reported for Si self-interstitial diffusion in SiO₂ (Ref. 50) and is explained by the emission of O vacancies (or SiO) from the interface (see also Sec. IV C).

B. Supposed mechanism of GeO diffusion in SiO₂

From our experiments GeO is identified as the mobile species in SiO₂, which explains both the correlated Ge redistribution and loss. But the diffusion mechanism deserves closer attention, as the idea of a diffusing GeO molecule through the SiO₂ network is probably misleading. At elevated temperatures ($T \geq 900^\circ\text{C}$), which are required for NC formation and oxide annealing, statistically breaking and reforming of Si—O bonds occurs within the SiO₂ network including bond switching during relaxation. Thus, it is likely that the GeO molecule is integrated into the covalent structure of SiO₂. In Figs. 13(a)–13(c) a possible configuration for embedded GeO in the SiO₂ network is schematically shown neglecting the real tetragonal structure of the oxide. The switching of two Si—O bonds leads to a structure similar to a so-called Ge oxygen-deficient center (Ge ODC) (Ref. 52) characterized by an oxygen vacancy (V_O) in combination with a substitutional Ge atom (S_{Ge}). Several possible models for an oxygen vacancy in SiO₂ are reported.^{51,53,54} A configuration as in Fig. 13(c) with three oxygen bonds and one Ge—Si bond corresponds to a Ge^{3+} oxidation state as obtained in the XPS spectra in Fig. 5:



Remember that with GeO also an extra O is introduced which migrates accompanied to the Ge ODC. But, along its way through the oxide, it is exchanged with oxygen from the relaxing SiO₂ network. If such a Ge ODC reaches the oxide surface, it emanates from the surface into the annealing ambient as a GeO molecule. In case O is present in the annealing ambient, the oxygen vacancy and thus the Ge ODC is annihilated, forming “immobile” GeO₂ which is embedded

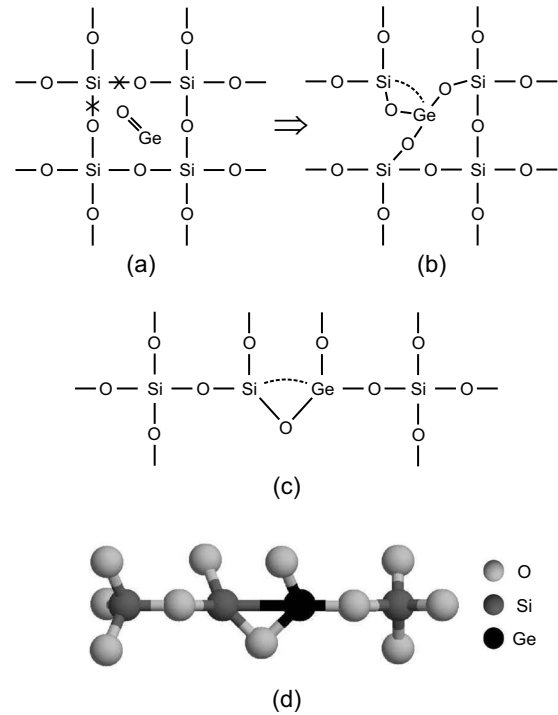
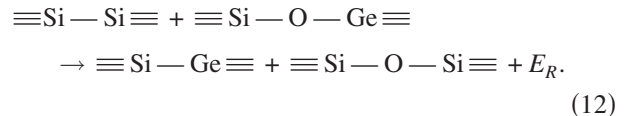


FIG. 13. Model for the introduction of a GeO molecule in the SiO₂ network. (a) Switching of two Si—O bonds (marked by crosses) leads to a reconfiguration as suggested in (b) by the formation of a bound Ge interstitial and an oxygen vacancy or to a probably more relaxed state as shown in (c). The latter configuration is similar to the triangular-oxygen-deficiency center in SiO₂ as proposed by Uchino *et al.* (Ref. 51) A 3D model of (c) is shown in (d), for instance, with an interatomic distance of 1.6 and 2.38 Å for Si—O and Si—Ge, respectively (Ref. 52), and a Si—O—Si (Ge—O—Si) bond angle of about 144°.

in SiO₂. This state corresponds to the fixed Ge amount closer to the oxide surface as shown in Fig. 10(a).

In the temperature range up to 1000 °C oxygen vacancies have a much higher mobility in SiO₂ than Si or Ge interstitials.^{53,55} Previous experiments reveal that in Ge doped silica glass only Ge ODC's are observed or, in other words, the oxygen vacancies localize preferably near Ge atoms.^{52,56} Si—Si related ODC's with neighboring Ge atoms are transformed in an exothermal reaction to Si—Ge related ones due the weaker Ge—O bond with an energy gain of $E_R \approx 0.6 \text{ eV}$:⁵²



The existence of such Ge related oxygen vacancy defects was confirmed at Ge implanted oxides by luminescence measurements.^{57,58} The process of enhanced Ge diffusivity is similar to the well known transient enhanced diffusion of boron, which is related to the diffusion of mobile Si self-interstitials in Si bulk material.⁵⁹ Here, the Ge impurity atom is connected to a highly mobile oxygen vacancy representing a diffusing Ge ODC complex. In that way the Ge atom gains

a much higher diffusivity than a Ge interstitial alone. Recent investigations by Minke *et al.*⁴⁸ show that the activation energies for the diffusion of Ge and Si in SiO₂ are nearly equivalent, which leads the authors to the suggestion that the diffusion mechanism is similar for both. Dangling bonds of the glassy matrix are supposed to be involved in the diffusion process instead of an Si or Ge interstitial motion. This clearly underlines the coherence of our model.

C. Role of Si/SiO₂ interface

The existence of a substoichiometric SiO_x ($x < 2$) region close to the Si/SiO₂ interface is well known and widely accepted in the microstructure of SiO₂ films on Si. This is equivalent to the presence of a high concentration of oxygen vacancies decaying with oxide depth.⁶⁰ The emission and diffusion of V_O is much more pronounced during annealing in an ambient with low or even negligible oxygen partial pressure.⁶¹ As the O vacancies are essentially involved in Ge ODC's (shown before), the mobility of the Ge increases with the number of available oxygen vacancies. This explains the enhanced Ge mobility with decreasing distance of the Ge profile to the Si/SiO₂ interface as obtained from Fig. 12. Our calculated values for the activation energy of Ge migration of $E_A \approx 0.95$ eV and $E_A \geq 1.55$ eV approximate the reported value of oxygen vacancy migration of $E_A = 1.8$ eV (Ref. 53) (from *ab initio* calculations according to an ideal oxide network) with increasing oxide thickness. Available oxygen vacancies support pathways for the Ge atoms diverging from the ideal model of oxygen vacancy migration. In the balance of energies a contribution of formation ($E_A = 0.85$ eV from *ab initio* calculations^{62,63}) can be omitted as the detachment of Ge atoms from Ge precipitates in SiO₂ (which form already during Ge implantation) is mediated by an exothermal reaction similar to an oxidation to GeO.

As a comparable effect, the self-diffusivity of Si in SiO₂ shows also a significant dependence on the oxide thickness.⁵⁰ The diffusivity increases with reduced oxide thickness, but this influence gets weaker if oxygen is introduced in the annealing ambient.^{49,50} SiO molecules are discussed to be involved in the Si self-diffusion.^{64–66} It was argued that, especially during annealing at very low oxygen partial pressure, SiO molecules are emitted from the Si/SiO₂ interface into the oxide.⁶¹ However, the explanation of the present results using GeO and SiO molecules instead of O vacancies leads to contradictions. The molecules would annihilate each other when they meet in the oxide region between the Ge profile and the Si/SiO₂ interface:



An unbound Ge interstitial would remain in SiO₂, which has a much lower diffusivity in SiO₂ than GeO as discussed before. The Ge diffusivity would tend to decrease with decreasing oxide thickness in contradiction to present results (Fig. 12). However, as mentioned by Stesmans *et al.*,⁵⁴ the model of SiO in SiO₂ can conceivably be unravelled by the idea of a Si—Si oxygen vacancy in accordance to our structure hypothesis:⁵¹

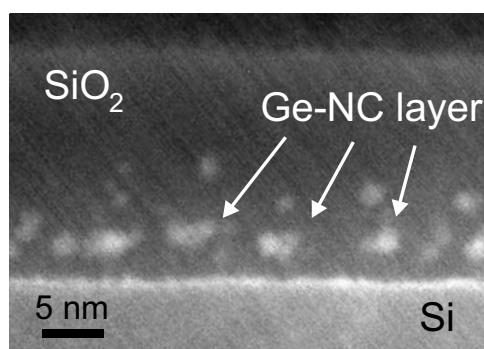
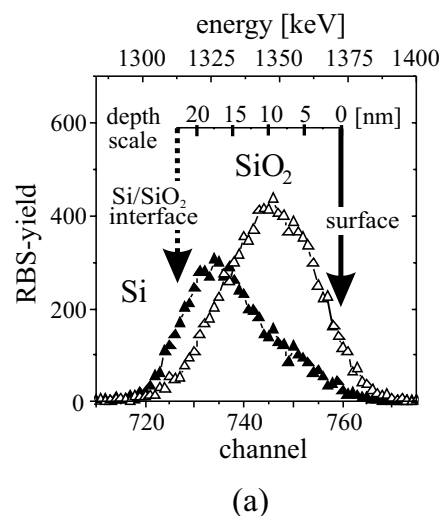


FIG. 14. Formation of a near-interface layer of Ge NC's in 20 nm SiO₂ after 5×10^{15} ⁷⁴Ge⁺-ions/cm² implantation at 12 keV and subsequent annealing (950 °C for 30 s in Ar). (a) RBS Ge spectra after ion implantation (Δ) and annealing (▲). After annealing the major part of the Ge ($\sim 1.3 \times 10^{15}$ cm⁻²) is located in vicinity to the Si/SiO₂ interface. A minor part is trapped at the Si substrate surface. (b) HAADF STEM image reveals separate Ge NC's of about 2 nm size, visible as bright spots, close to the Si/SiO₂ interface and some individual in the oxide bulk.



Migrating oxygen vacancies cause long-range distortions in the oxide network⁵² leading actually to a Si self-diffusion in SiO₂. Penetrating oxygen in SiO₂ from the annealing ambient annihilates the oxygen vacancies and suppresses the Si self-diffusion. Thus, the Si self-diffusion in SiO₂ can be explained by a mechanism involving oxygen vacancies instead of SiO molecules or Si interstitials.

V. CONSEQUENCES OF THE Ge LOSS AND REDISTRIBUTION FOR A Ge NANOCRYSTAL MEMORY DEVICE

The significant mobility of Ge can be used for the formation of a self-organized Ge NC layer close to Si/SiO₂ interface which has been reported for Ge implanted gate oxides of

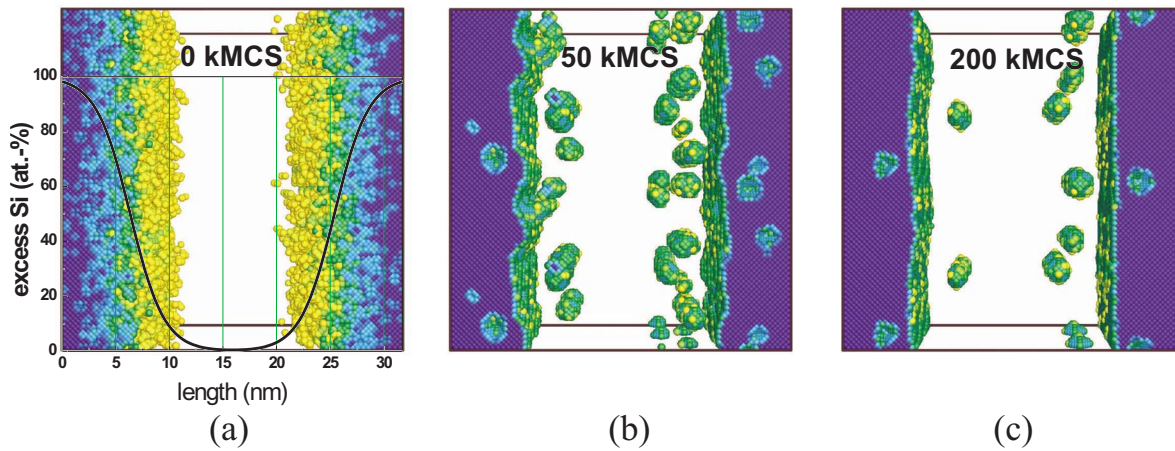


FIG. 15. (Color online) Formation of a Si NC layer close to the Si/SiO₂ interface traced by 3D-KLMC simulation for a stack of 50 nm *n*⁺-poly Si/15 nm SiO₂/(100)Si which is irradiated by 50 keV, 1×10^{16} Si⁺-ions/cm². The gray scale/color reflects the number of diatomic Si—Si bonds. After 50 000 MC steps Si NC's and SiO₂ clusters are formed in the SiO₂ and the Si bulk, respectively. Due to the higher mobility of O in Si than Si in SiO₂ the Si NC's are far more stable than the SiO₂ clusters in Si. With proceeding simulation/annealing time the Si/SiO₂ interface gets smoother and the NC's dissolve until an equilibrium of totally separated regions (SiO₂ and Si bulks) is reached. The KMC simulation was performed by Heinig, Forschungszentrum Dresden-Rossendorf, and is presented with kind permission of the author and the publisher (Ref. 3, © by Springer, Berlin, 2005) (see also Refs. 67–69).

100 nm¹⁰ or more device relevant of 20 nm thickness.^{9,18} Such a near-interface NC layer is a desired configuration for Ge-nanocrystal-based memory devices.^{3,4,9,11} The Ge redistribution due to volatile GeO or, in other words, due to Ge ODC's during annealing in Ge implanted SiO₂ ($d_{\text{ox}} = 20$ nm) is illustrated in Fig. 14(a). The Ge loss, mainly occurring at the near-surface region, is about 30% of the implanted fluence after annealing at 950 °C for 30 s.

Contrary to the Ge accumulation at the uppermost Si substrate shown in Fig. 12, here the Ge forms NC's within the oxide which is confirmed by TEM [Fig. 14(b)]. This process deserves a more detailed description. For IBS in thin gate oxides ($d_{\text{ox}} \leq 20$ nm), the implantation cascade usually meets the Si substrate resulting in a mixing of the Si/SiO₂ interface. During subsequent annealing (phase) separation of Si and SiO₂ occurs associated with a complete interface reconstruction and a formation of tiny Si precipitates in the SiO₂ close to the Si/SiO₂ interface.⁷⁰ At these Si precipitates a significant amount of mobile Ge (from GeO) condenses [see Eq. (9)]. The high contrast of the bright spots in the TEM micrograph of Fig. 14 confirms that the NC's are composed mostly of Ge atoms, as such small Si NC's would be not resolvable by high-angle annual dark field (HAADF) scanning TEM. On the contrary, to Ge interstitial diffusion, the migration of GeO-like complexes lead to an oxidation of the excess Si in SiO₂, confirming the formation of a nearly elementary pure Ge NC's layer.

The process of interface reconstruction and formation of Si precipitates (or even NC's) in the oxide can be traced in a 3D-KLMC simulation as presented in Fig. 15.³ As a model system, there a Si/SiO₂/Si stack is treated by a Si irradiation. The Si excess in the oxide close to the Si/SiO₂ interfaces is achieved just by ion beam mixing, more or less independent of the kind of the implanted ions. During annealing the interfaces recover and a certain amount of mixed Si atoms remain within the SiO₂, forming precipitates that subsequently grow to Si NC's.

The influence of mobile Ge has to be carefully adjusted according to the right balance in processing between the presence of excess oxygen necessary for the Ge redistribution and the Ge loss, especially if a single NC layer is desired. In addition to appropriate implantation conditions, special care has to be taken for the oxygen partial pressure in the annealing ambient which has to be quite low; otherwise GeO₂ formation in the gate oxide dominates. A small amount of hydrogen in the annealing ambient can be used to suppress the Ge loss. In addition subsequent thermal processes during device fabrication including hydrogen or oxygen containing species and/or post-IBS heat treatments may influence the NC's arrangement. The deposition of a capping layer such as Si₃N₄ prior to implantation is not helpful because in this case oxygen from moisture is excluded which is needed for a considerable Ge redistribution.

VI. SUMMARY

A considerable Ge loss and redistribution is obtained during cleaning and annealing treatment of low-energy Ge implanted SiO₂ films, whereas the loss becomes more pronounced the closer the implanted profile is located to the oxide surface. A model for the diffusion of Ge in SiO₂ is given, which explains the high mobility of Ge in the oxide during annealing considering oxygen vacancies as the key diffusing elements. Ge loss and redistribution are strongly correlated to (i) a spatial modification of the oxide stoichiometry due to atomic relocations during ion implantation and (ii) the penetration of additional oxygen and hydrogen species into the damaged oxide after implantation. Atomic collision during Ge implantation leads to a near surface oxygen deficit (i.e., Si enrichment) and an oxygen excess slightly behind the Ge implanted profile with respect to the initial SiO₂ stoichiometry. Additionally, moisture (H₂O vapor, H, and OH) penetrates into the damaged oxide during storage at

air, compensates a Si excess close to the oxide surface, and enhances the oxygen excess in further depth. Thus, depending on the implantation parameters the overall oxygen (and hydrogen) excess in SiO₂ (“intrinsic source”) is already conditioned prior to annealing. Apart from very shallow Ge profiles, where H₂O₂ containing cleaning chemicals cause a drastic reduction of the Ge content in the oxide by the formation of water soluble compounds (GeO₂, H₂GeO₃), the main Ge loss and redistribution occurs during subsequent annealing treatment. For neutral annealing ambients (e.g., Ar) the local ratio of Ge and excess oxygen within the oxide after ion implantation and cleaning determines whether Ge is incorporated in the SiO₂ network as GeO₂, oxidizes to highly mobile GeO, or remains as elemental Ge forming Ge NC’s. A small amount of oxygen in the annealing ambient assists the formation of GeO and GeO₂, whereas an H₂/Ar annealing at 900 °C significantly reduces the Ge loss probably due to a reduction of Ge oxides. During annealing the Ge loss is related to mobile GeO, which diffuses toward the oxide surface and escapes there into the annealing ambient (or the vacuum) due to its high vapor pressure. The diffusivity of GeO in SiO₂ ($D > 10^{-16}$ cm²/s at 900 °C) is orders of magnitude higher than of Ge interstitials. These considerations agree with the experimental result¹⁵ that the Ge redistribution

in SiO₂ is highly suppressed for samples protected by a diffusion barrier (e.g., Si₃N₄) prior to implantation avoiding a penetration of the damaged oxide by moisture or oxygen. GeO molecules in SiO₂ can be considered to be equivalent to Ge ODC’s. Then, the diffusion mechanism is determined by the correlated Ge and oxygen vacancy movement through the oxide. As the Si/SiO₂ interface acts as an additional source of oxygen vacancies, the diffusivity of Ge is influenced by the oxide thickness, too.

Although a Ge loss is an undesired effect, with our findings and the diffusion model the high Ge mobility can advantageously be used to form a near interface, δ -like Ge NC’s layer in thin gate oxides for multidot memory devices. The diffusing Ge is trapped at Si nucleation centers close to the Si/SiO₂ interface that are formed as a result of interface mixing and phase separation during ion implantation and annealing, respectively.

ACKNOWLEDGMENTS

Special thanks to R. Grötzschel, M. Beckers (RBS), D. Grambole (NRA), and H. Reuther (XPS) for analysis support, to T. Müller for TRIDYN assistance, and to the FZD implanter and cleanroom teams for sample preparation.

*v.beyer@fzd.de

¹2003 edition of the ITRS, <http://public.itrs.net/>

²S. Tiwari, F. Rana, H. Hanafi, A. Hartstein, E. F. Crabbé, and K. Chan, *Appl. Phys. Lett.* **68**, 1377 (1996).

³V. Beyer and J. von Borany, in *Materials for Information Technologies*, edited by E. Zschech, C. Whelan, and T. Mikolajick (Springer, Berlin, 2005), pp. 139–147.

⁴H. I. Hanafi, S. Tiwari, and I. Khan, *IEEE Trans. Electron Devices* **43**, 1553 (1996).

⁵P. Dimitrakis *et al.*, *Solid-State Electron.* **48**, 1511 (2004).

⁶J. von Borany, T. Gebel, K.-H. Stegemann, H.-J. Thees, and M. Wittmaack, *Solid-State Electron.* **46**, 1729 (2002).

⁷B. Schmidt, K.-H. Heinig, L. Röntzsch, T. Müller, K.-H. Stegemann, and E. Votintseva, *Nucl. Instrum. Methods Phys. Res. B* **242**, 146 (2006).

⁸J. De Blauwe, *IEEE Trans. Nanotechnol.* **1**, 72 (2002).

⁹V. Beyer, J. von Borany, and M. Klimenkov, *Appl. Phys. Lett.* **89**, 193505 (2006).

¹⁰J. von Borany, R. Grötzschel, K.-H. Heinig, A. Markwitz, B. Schmidt, W. Skorupa, and H.-J. Thees, *Solid-State Electron.* **43**, 1159 (1999).

¹¹H.-J. Thees, M. Wittmaack, K.-H. Stegemann, J. von Borany, K.-H. Heinig, and T. Gebel, *Microelectron. Reliab.* **40**, 867 (2000).

¹²S. Duguay, J. J. Grob, A. Slaoui, Y. L. Gall, and M. Amann-Liess, *J. Appl. Phys.* **97**, 104330 (2005).

¹³J. von Borany, R. Grötzschel, K. H. Heinig, A. Markwitz, W. Matz, B. Schmidt, and W. Skorupa, *Appl. Phys. Lett.* **71**, 3215 (1997).

¹⁴A. Markwitz, B. Schmidt, W. Matz, R. Grötzschel, and A. Mücklich, *Nucl. Instrum. Methods Phys. Res. B* **142**, 338 (1998).

¹⁵K. H. Heinig, B. Schmidt, A. Markwitz, R. Grötzschel, M. Strobel, and S. Oswald, *Nucl. Instrum. Methods Phys. Res. B* **148**, 969 (1999).

¹⁶V. Borodin, K.-H. Heinig, and B. Schmidt, *Nucl. Instrum. Methods Phys. Res. B* **147**, 286 (1999).

¹⁷S. Oswald, B. Schmidt, and K.-H. Heinig, *Surf. Interface Anal.* **29**, 249 (2000).

¹⁸M. Klimenkov, J. von Borany, W. Matz, R. Grötzschel, and F. Herrmann, *J. Appl. Phys.* **91**, 10062 (2002).

¹⁹E. S. Marstein, A. E. Gunnæs, A. Olsen, T. G. Finstad, R. Turan, and U. Serincan, *J. Appl. Phys.* **96**, 4308 (2004).

²⁰B. Schmidt, D. Grambole, and F. Herrmann, *Nucl. Instrum. Methods Phys. Res. B* **191**, 482 (2002).

²¹A. Markwitz, W. Matz, B. Schmidt, and R. Grötzschel, *Surf. Interface Anal.* **26**, 359 (1998).

²²W. Rudolph, C. Bauer, K. Brankoff, D. Grambole, R. Grötzschel, C. Heiser, and F. Herrmann, *Nucl. Instrum. Methods Phys. Res. B* **15**, 508 (1986).

²³S. Tanuma, C. Powell, and D. Penn, *Surf. Sci.* **192**, L849 (1987).

²⁴S. Oswald, B. Schmidt, and K.-H. Heinig, *Cryst. Res. Technol.* **40**, 1134 (2005).

²⁵W. Möller and W. Eckstein, *Nucl. Instrum. Methods Phys. Res. B* **2**, 814 (1984).

²⁶SRIM program is free for download at <http://www.srim.org>

²⁷J. Oh and J. C. Campbell, *J. Electron. Mater.* **33**, 364 (2004).

²⁸K. Prabhakaran, F. Maeda, Y. Watanabe, and T. Ogino, *Thin Solid Films* **369**, 289 (2000).

²⁹D. Schmeisser, R. D. Schnell, A. Bogen, F. J. Himpsel, D. Rieger, G. Landgren, and J. F. Morar, *Surf. Sci.* **172**, 455 (1986).

³⁰J. Zuk, H. Krzyzanowska, M. J. Clouter, M. B. H. Bubert, L.

- Rebohle, and W. Skorupa, *J. Appl. Phys.* **96**, 4952 (2004).
- ³¹W. K. Choi, V. Ho, V. Ng, Y. W. Ho, S. P. Ng, and W. K. Chim, *Appl. Phys. Lett.* **86**, 143114 (2005).
- ³²R. Meyer and E. E. Pietsch, *Gmelins Handbuch der Anorganischen Chemie*, 8th ed. (Verlag Chemie, GmbH, Weinheim/Bergstrasse, 1958), Vol. 45, Chap. Germanium (Ergänzungsband), pp. 32–33,457,493,502–506.
- ³³W. W. Harvey and H. C. Gatos, *J. Electrochem. Soc.* **105**, 654 (1958).
- ³⁴G. W. Arnold, G. D. Marchi, P. Mazzoldi, and G. Battaglin, *Nucl. Instrum. Methods Phys. Res. B* **116**, 364 (1996).
- ³⁵R. A. B. Devine, *Nucl. Instrum. Methods Phys. Res. B* **91**, 378 (1994).
- ³⁶T. A. Michalske and B. C. Bunker, *J. Appl. Phys.* **56**, 2686 (1984).
- ³⁷*CRC Handbook of Chemistry and Physics*, edited by D. R. Lide, 82nd ed. (CRC Press, Boca Roton, FL, 2001).
- ³⁸W. Bues and H. v. Wartenberg, *Z. Anorg. Allg. Chem.* **266**, 281 (1951).
- ³⁹W. L. Jolly and W. M. Latimer, *J. Am. Chem. Soc.* **74**, 5757 (1952).
- ⁴⁰E. K. Kazenas, M. A. Bol'shikh, and A. A. Petrov, *Russ. Metall.* **3**, 16 (1996).
- ⁴¹S. Ciraci and H. Wagner, *Phys. Rev. B* **27**, 5180 (1983).
- ⁴²S. J. Jung, J. Y. Lee, S. Hong, and S. Kim, *J. Phys. Chem. B* **109**, 24445 (2005).
- ⁴³C. U. S. Larsson and A. S. Flodström, *Phys. Rev. B* **43**, 9281 (1991).
- ⁴⁴J.-H. Cho, L. Kleinman, K.-J. Jin, and K. S. Kim, *Phys. Rev. B* **66**, 113306 (2002).
- ⁴⁵D. Schmeisser, F. J. Himpsel, and G. Hollinger, *Phys. Rev. B* **27**, 7813 (1983).
- ⁴⁶J. Dalla Torre, J.-L. Bocquet, Y. Limoge, J.-P. Crocombette, E. Adam, G. Martin, T. Baron, P. Rivallin, and P. Mur, *J. Appl. Phys.* **92**, 1084 (2002).
- ⁴⁷G. Taraschi, S. Saini, W. W. Fan, L. C. Kimerling, and E. A. Fitzgerald, *J. Appl. Phys.* **93**, 9988 (2003).
- ⁴⁸M. V. Minke and K. A. Jackson, *J. Non-Cryst. Solids* **351**, 2310 (2005).
- ⁴⁹D. Mathiot, J. P. Schunck, M. Perego, M. Fanciulli, P. Normand, C. Tsamis, and D. Tsoukalas, *J. Appl. Phys.* **94**, 2136 (2003).
- ⁵⁰S. Fukatsu, T. Takahashi, K. M. Itoh, M. Uematsu, A. Fujiwara, H. Kageshima, Y. Takahashi, K. Shiraishi, and U. Gösele, *Appl. Phys. Lett.* **83**, 3897 (2003).
- ⁵¹T. Uchino, M. Takahashi, and T. Yoko, *Phys. Rev. B* **62**, 2983 (2000).
- ⁵²V. B. Sulimov, P. V. Sushko, A. H. Edwards, A. L. Shluger, and A. M. Stoneham, *Phys. Rev. B* **66**, 024108 (2002).
- ⁵³J. Song, L. R. Corrales, G. Kresse, and H. Jonsson, *Phys. Rev. B* **64**, 134102 (2001).
- ⁵⁴A. Stesmans, B. Nouwen, and V. V. Afanas'ev, *Phys. Rev. B* **66**, 045307 (2002).
- ⁵⁵K. A. Jackson, *Kinetic Processes* (Wiley-VCH Verlag, Weinheim, 2004).
- ⁵⁶C. M. Carbonaro, V. Fiorentini, and F. Bernardini, *Phys. Rev. B* **66**, 233201 (2002).
- ⁵⁷L. Rebohle, J. von Borany, R. A. Yankov, W. Skorupa, I. E. Tyschenko, H. Fröb, and K. Leo, *Appl. Phys. Lett.* **71**, 2809 (1997).
- ⁵⁸L. Rebohle, J. von Borany, H. Fröb, T. Gebel, M. Helm, and W. Skorupa, *Nucl. Instrum. Methods Phys. Res. B* **188**, 28 (2002).
- ⁵⁹A. Agarwal, H.-J. Gossmann, and D. J. Eaglesham, *Appl. Phys. Lett.* **74**, 2331 (1999).
- ⁶⁰R. Devine, W. Warren, J. Xu, I. Wilson, P. Paillet, and J.-L. Leray, *J. Appl. Phys.* **77**, 175 (1995).
- ⁶¹Y. Takakuwa, M. Nihei, and N. Miyamoto, *Jpn. J. Appl. Phys., Part 2* **32**, L480 (1993).
- ⁶²N. Capron and G. Boureau, *J. Chem. Phys.* **117**, 1843 (2002).
- ⁶³P. E. Blöchl, *Phys. Rev. B* **62**, 6158 (2000).
- ⁶⁴D. Tsoukalas, C. Tsamis, and P. Normand, *J. Appl. Phys.* **89**, 7809 (2001).
- ⁶⁵D. Tsoukalas and C. Tsamis, *Appl. Phys. Lett.* **63**, 3167 (1993).
- ⁶⁶M. Uematsu, H. Kageshima, Y. Takahashi, S. Fukatsu, K. M. Itoh, K. Shiraishi, and U. Gösele, *Appl. Phys. Lett.* **84**, 876 (2004).
- ⁶⁷S. Reiss and K.-H. Heinig, *Nucl. Instrum. Methods Phys. Res. B* **102**, 256 (1995).
- ⁶⁸T. Müller, K.-H. Heinig, and W. Möller, *Appl. Phys. Lett.* **81**, 3049 (2002).
- ⁶⁹M. Strobel, K.-H. Heinig, W. Möller, A. Meldrum, D. Zhou, C. White, and R. Zuhr, *Nucl. Instrum. Methods Phys. Res. B* **147**, 343 (1999).
- ⁷⁰K. H. Heinig, T. Müller, B. Schmidt, M. Strobel, and W. Möller, *Appl. Phys. A: Mater. Sci. Process.* **77**, 17 (2003).